Numerical Evaluating the Permeability of Rocks Based on Correlation Dependence on Geometry

Vadim Lisitsa[1], Tatyana Khachkova[2(✉)], Oleg Sotnikov[3], Ilshat Islamov[3], and Dinis Ganiev[3]

[1] Institute of Mathematics SB RAS, Koptug Avenue 4, Novosibirsk 630090, Russia
lisitsavv@ipgg.sbras.ru
[2] Institute of Petroleum Geology and Geophysics SB RAS, Koptug Avenue 3, Novosibirsk 630090, Russia
khachkovats@ipgg.sbras.ru
[3] TatNIPIneft Institute, PJSC Tatneft named after V.D. Shashin, M. Dgalilya st. 32, Bugulma, Tatarstan 423230, Russia

Abstract. We present a resource-saving algorithm for numerical evaluation of the absolute permeability of a rock from the sample's CT-images of huge size, which makes it possible to perform such an assessment using limited computing resources, in particular, personal computers. It is based on a decomposition of the 3D sample image into small representative sub-samples, for which the absolute permeability is estimated based on the numerical solution of the Stokes equation in a static formulation, followed by a creation of the functional dependencies between the permeability and open porosity. After that these dependencies can be extended to the entire original sample or to the full-sized core sample.

Keywords: Permeability · numerical estimation · porosity · correlation dependence · scaling · digital rock physics · CT-images

1 Introduction

Digital rock physics is a modern field of computational physics used to simulate various processes at the scale of rocks pores. The models of rock including the pore space and the rock skeleton are built from 3D CT-images with using different image segmentation methods [1]. The result is a three-dimensional grid model with a finite (small) number of different components representing different fluids in the pore space or minerals in the skeleton. After that, for each voxel the appropriate physical properties are assigned and the required physical field is calculated.

T. Khachkova performed numerical simulation within the FNI project FWZZ-2022-0022. V. Lisitsa constructed trends and made estimates under the support of RSCF grant no. 21-71-20003.

© The Author(s), under exclusive license to Springer Nature Switzerland AG 2023
O. Gervasi et al. (Eds.): ICCSA 2023 Workshops, LNCS 14106, pp. 91–102, 2023.
https://doi.org/10.1007/978-3-031-37111-0_7

One of the main areas of digital rock physics is the upscaling properties of rocks for their further using in macroscale models. In particular, numerical upscaling is widely used to estimate the absolute and relative permeability [2,6,7,14,17], elastic parameters [9,10,19], electrical resistivity [2,13,16] and many other parameters. At the same time, the size and resolution of tomographic images are determined by the apparatus [15], in particular, modern microtomographs make it possible to obtain an image with a resolution up to 0.5 micron per voxel and a size up to 4000 voxels in each direction. So the working image size without edge effects is about 2000 voxels. As a result, the computational grid for problems is about $10^9 - 10^{10}$ points. At the same time, the physical sizes of the computational domain are the first millimeters, which, of course, raises the question of representativeness of the considered volume [4]. In this work it is shown that the geometric characteristics of the pore space are determined quite stably on the indicated dimensions, however, these dimensions are often insufficient for evaluation of the physical properties of the samples. Therefore, at present, the methods of computational rocks physics are applied to solve the set of problems for different sample sizes and to accumulate statistical data [11]. An alternative direction is geostatistical modeling of rock samples using multi-point statistics, or machine learning methods [12]. The first approach is more common, which is mainly related to the computational aspects of the tasks being decided. Solving a series of independent problems with the accumulation of statistics is an example of parallelization by tasks, where the scalability of the algorithm is 100%, i.e. there is no loss on overhead transactions and data exchange. At the same time, the size of each task allows you to perform simulation using a small number of graphics co-processors (GPUs), opening up the possibility of modeling at workstations, which is relevant for geophysical laboratories with limited access to computing resources [8]. This paper develops the approach proposed in [11], which proposes to accumulate statistics on a large set of subsamples with subsequent construction of functional dependencies between the estimated parameters and sample porosity.

2 Evaluating the Absolute Permeability of Rock

2.1 Mathematical Statement of the Problem

To evaluate the absolute permeability of rock it is necessary to calculate the steady-state flow of a viscous incompressible fluid in a pore space. We've got the model of the rock sample obtained by binary segmentation of CT-images. Formally, the mathematical statement of the problem is as follows. The stationary Stokes equation is considered:

$$\begin{aligned} \mu \Delta \vec{u} - \nabla p = 0, \\ \nabla \cdot \vec{u} = 0, \end{aligned} \tag{1}$$

defined in the pore space

$$\Omega_p \subseteq \Omega = [0, X_1] \times [0, X_2] \times [0, X_3],$$

where $\vec{u} = \vec{u}(\vec{x})$ is the velocity vector of fluid flow, $p = p(\vec{x})$ is the pressure, μ is the fluid viscosity. On two opposite sides of the computational domain, the pressure values are assumed to be defined, and the tangential velocity components are equal to zero:

$$\begin{aligned} p(\vec{x})\big|_{x_1=0} &= p_0, \qquad & p(\vec{x})|_{x_1=X_1} &= p_1, \\ \vec{u} \times \vec{n}\big|_{x_1=0} &= 0, \qquad & \vec{u} \times \vec{n}\big|_{x_1=X_1} &= 0, \end{aligned}$$

where x_1 is the spatial coordinate in the direction of pressure changing. The adhesion conditions are defined at the outer boundaries and at the boundary between the pore space and rock matrix:

$$\vec{u}\big|_B = 0.$$

The solution of Stokes Eq. (1) determines the fluid velocity field and the pressure distribution. So the fluid flow through the sample can then be calculated as:

$$Q_x = \int_0^{X_2} \int_0^{X_3} u_1 dx_2 dx_3,$$

where Q_x is the fluid flow, u_1 is the flow velocity in the direction of pressure changing.

On the other hand, the fluid flow in a porous medium satisfies the Darcy equation:

$$Q_x = -\frac{S\kappa}{\mu} \frac{(p_1 - p_0)}{X_1},$$

where $S = X_2 X_3$ is the cross-sectional area of the sample, κ is the absolute permeability. As a result, knowing the fluid flow through the sample at a given pressure drop, the permeability can be estimated as

$$\kappa = -\frac{\mu X_1}{(p_1 - p_0)S} Q_x,$$

The solution of the Stokes equation is the main part of the absolute permeability estimation algorithm. To construct a stationary solution, the method of establishment is used, namely, the solution of the Stokes equation is constructed as an asymptotic steady-state solution of the non-stationary Navier-Stokes equation, in which the influence of convective terms is neglected due to the low flow velocity:

$$\begin{gathered} \frac{\partial \vec{u}}{\partial t} = -\nabla p + \mu \Delta \vec{u}, \\ \nabla \cdot \vec{u} = 0, \end{gathered}$$

Here it is necessary to supplement the problem with initial conditions, which are assumed to be zero.

2.2 Numerical Solution of the Navier-Stokes Equation

For the numerical solution of the Navier-Stokes equation, the projection method is used, the essence of which is a two-stage calculation of the solution. Let the solution at the time layer $t^n = n\tau$ is defined, and it is necessary to calculate the solution at the layer t^{n+1}. At the first step of the algorithm, a preliminary calculation of the speed is carried out, which may not satisfy the continuity equation. In the second step, the pressure is calculated to provide the necessary velocity correction to satisfy the continuity equation, after which the velocity is corrected.

$$\begin{gathered}\frac{\vec{u}^*-\vec{u}^n}{dt} = \mu\Delta\vec{u}^n,\\ \frac{\vec{u}^{n+1}-\vec{u}^*}{dt} = -\nabla p^{n+1},\\ \nabla\cdot\vec{u}^{n+1} = 0,\end{gathered}$$

where $\vec{u}^n$, $\vec{u}^{n+1}$ are the velocities at the time layers t^n and t^{n+1} accordingly, $\vec{u}^*$ - auxiliary velocity vector, p^{n+1} is the pressure in the fluid at the time layer t^{n+1}.

From the last two equations, one can get:

$$\begin{gathered}\frac{\vec{u}^*-\vec{u}^n}{dt} = \mu\Delta\vec{u}^n,\\ \Delta p^{n+1} = \frac{\nabla\cdot\vec{u}^*}{dt},\\ \frac{\vec{u}^{n+1}-\vec{u}^*}{dt} = -\nabla p^{n+1}.\end{gathered}$$

This equations system determines the projection method for solving the Navier-Stokes equation. It can be seen that the prediction and correction of the velocity is carried out by a method, which is explicit in time, while the correction of pressure requires the solution of the Poisson equation in the pore space.

Spatial discretization is based on the finite difference method using a staggered grid scheme. Grid functions are defined as

$$\begin{gathered}p_{i,j,k} = p(ih_1, jh_2, kh_3), \qquad (u_1)_{i+1/2,j,k} = u_1((i+1/2)h_1, jh_2, kh_3),\\ (u_2)_{i,j+1/2,k} = u_2(ih_1, (j+1/2)h_2, kh_3),\ (u_3)_{i,j,k+1/2} = u_3(ih_1, jh_2, (k+1/2)h_3),\end{gathered}$$

where h_1, h_2, h_3 are the spatial grid steps, i, j, k are the ordinal numbers of the grid cell. Further, it can be used the operators that approximate second-order differential operators:

$$\begin{gathered}L[f]_{I,J,K} = D_1^2[f]_{I,J,K} + D_2^2[f]_{I,J,K} + D_3^2[f]_{I,J,K} = \Delta f + O(h^2),\\ D_1^2[f]_{I,J,K} = \frac{f_{I+1,J,K}-2f_{I,J,K}+f_{I-1,J,K}}{h_1^2} = \left.\frac{\partial^2 f}{\partial x_1^2}\right|_{I,J,K} + O(h_1^2),\\ D_1^c[f]_{I,J,K} = \frac{f_{I+1/2,J,K}-f_{I-1/2,J,K}}{h_1} = \left.\frac{\partial f}{\partial x_1}\right|_{I,J,K} + O(h_1^2),\end{gathered}$$

where L is a finite-difference operator approximating the Laplace operator, f is a sufficiently smooth function, D_1^c, D_2^c, D_3^c are finite-difference operators approximating the first spatial derivatives, D_1^2, D_2^2, D_3^2 are finite-difference operators approximating the second spatial derivatives. Here indices written in capital letters can take both integer and half-integer values. By appropriately substituting

indices, one can obtain operators that approximate derivatives in other spatial directions.

Using the introduced notation, the approximation of the Navier-Stokes equations (projection method) can be written as:

$$\begin{gathered}
\frac{(u_1^*)_{i+1/2,j,k}-(u_1^n)_{i+1/2,j,k}}{\tau}+\mu L[u_1^n]_{i+1/2,j,k}=0,\\
\frac{(u_2^*)_{i,j+1/2,k}-(u_2^n)_{i,j+1/2,k}}{\tau}+\mu L[u_2^n]_{i,j+1/2,k}=0,\\
\frac{(u_3^*)_{i,j,k+1/2}-(u_3^n)_{i,j,k+1/2}}{\tau}+\mu L[u_3^n]_{i,j,k+1/2}=0,\\
L[p^{n+1}]_{i,j,k}=\frac{D_1^c[u_1^*]_{i,j,k}+D_2^c[u_2^*]_{i,j,k}+D_3^c[u_3^*]_{i,j,k}}{\tau},
\end{gathered}$$

$$\frac{(u_1^{n+1})_{i+1/2,j,k}-(u_1^*)_{i+1/2,j,k}}{\tau}-D_1^c[p^{n+1}]_{i+1/2,j,k}=0,$$

$$\begin{gathered}
\frac{(u_2^{n+1})_{i,j+1/2,k}-(u_2^*)_{i,j+1/2,k}}{\tau}-D_2^c[p^{n+1}]_{i,j+1/2,k}=0,\\
\frac{(u_3^{n+1})_{i,j,k+1/2}-(u_3^*)_{i,j,k+1/2}}{\tau}-D_3^c[p^{n+1}]_{i,j,k+1/2}=0.
\end{gathered}$$

2.3 Algorithm Verification

To verify the algorithm, we considered a model for which an analytical solution is known. We considered impermeable samples with a cylindrical channel of circular cross section connecting opposite faces of the sample. In this case, there is an analytical solution of the Stokes equation, which makes it possible to construct the flow and estimate the absolute permeability

$$k=\frac{\pi R^4}{8S},$$

where k is the absolute permeability, R is the radius of the cylindrical channel and S is cross-sectional area of the sample.

The experiments were carried out for a fixed sample size equal to 80^3 voxels. The grid step was chosen equal to 1 m, the hole radius varied from 5 to 40 points (the limiting case implied impermeable side boundaries, where the channel touched the model boundaries). The simulation results are shown in Table 1.

Table 1. Verification of the permeability estimation algorithm. Results for a model with a cylindrical channel.

Hole radius	Theoretical evaluation	Simulation result	Relative error
5	0.038348	0.039277	2.4234%
10	0.613574	0.620464	1.123%
20	9.817187	9.870730	0.5454%
40	157.075	157.4713	0.2523%

3 Evaluation by Trend Using the Correlation Dependence on Geometry

In this study, we are based on the research performed by [11], which states that it is important not just to obtain fixed values of permeability or other parameters for a particular sample, but to reconstruct the statistical trends between geometry parameter (for example, porosity) and evaluated parameter, which is the absolute permeability in our case. In our research, we use the assumption that the total sample is large enough to be divided into representative sub-samples, at least, for the pore space geometry. As a result, we can evaluate the absolute permeability independently for each sub-sample and then construct correlation dependence between the permeability and porosity. So the estimated permeability can then be expanded to the total sample, full-sized core sample and so on.

3.1 Limestone Images Description

We consider four samples of limestone of the Medium Carboniferous system. They were originally cylindrical, with a length of 4 cm and a diameter of 3 cm. These samples were tested for porosity (through the fluid saturation method) and absolute permeability. Following that, the cubical sub-samples of 2 cm in size were taken out and specified measurements were performed. Later, the tiniest cubical sub-samples of 0.4 cm in size were extracted and scanned. It should be noted that the porosity of the smallest samples was also tested, but the permeability was not measured for them. As for the measurement error, when assessing porosity, it was 0.008–0.022% for cylindrical samples, 0.034–0.115% for medium samples and 4.567–11.27% for smallest samples. Table 2 shows the results of the laboratory measurements.

Table 2. The results of the laboratory measurements for the samples of various sizes.

Sample size	Sample No.	Porosity	Permeability (mD)		
			X	Y	Z
Large cylindrical	s07	0.156	26.3		
	s25	0.159	16.99		
	s31	0.191	40.93		
	s78	0.232	1684.10		
Medium cubical	s07	0.152	8.27	6.67	1.39
	s25	0.161	24.92	24.61	15.53
	s31	0.185	20.66	19.71	18.78
	s78	0.255	2527.7	2425.5	2243.9
Small cubical	s07	0.201	–		
	s25	0.128	–		
	s31	0.180	–		
	s78	0.288	–		

As we mentioned, the smallest samples were scanned, the resolution of CT-tomography was 3 μm per voxel and the sizes of obtained images were 1600–1800 voxels in each direction. After image pre-processing, including cropping to a region that lies completely within the target, non-correlated noise suppression based on the non-local mean Gauss filter method [5], and image segmentation by Otsu method [18] to separate the pore space and rock matrix without taking into account its mineral composition, we've obtained images of 1200^3 voxels, the cross-sections of which are shown in Fig. 1.

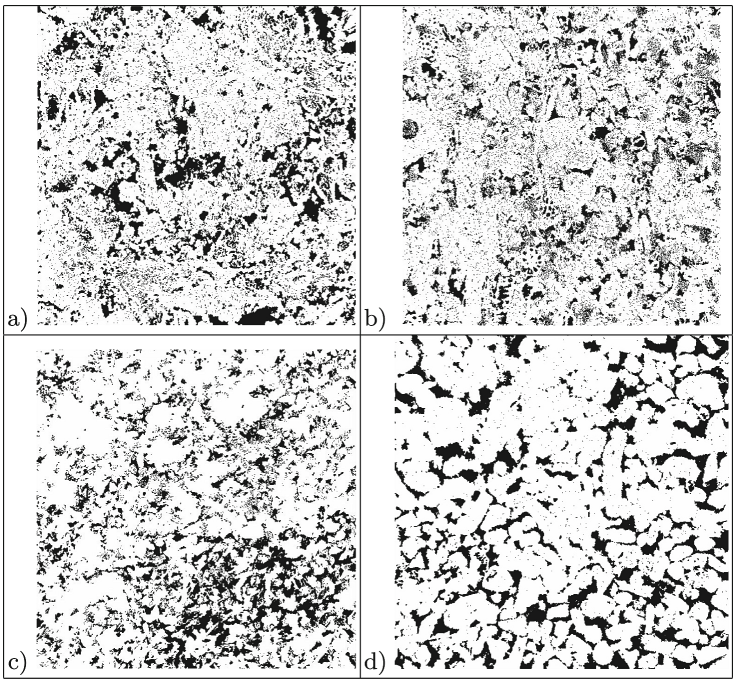


Fig. 1. 2D sections of the segmented images for the samples: a) no. 7; b) no. 25; c) no. 31; d) no. 78.

3.2 Methodology of Estimation

For numerical simulations, each sample was divided into 216 non-overlapping cubic sub-samples of 200^3 voxels, that is, the division occurred into 6 parts in each direction. This size of sub-sample was chosen taking into account the memory limitations of the GPU (nVidia GeForce 2090Ti with 12 GB of RAM). Then for each sub-sample, we calculated the total and open porosity, as well as the mean and standard deviation for these parameters over an ensemble of sub-samples. Note that the total porosity of the sample is defined as the ratio of the number of voxels corresponding to the pore space to the total number of voxels. Connected porosity includes only pores that form through channels connecting

opposite faces of the sample. That is, those pores that provide percolation of the sample. Moreover, the open porosity was calculated for each direction. The results of calculation are shown in Table 3. Here ϕ, ϕ_o are the porosity and open porosity respectively, $<>$ is the mean value and σ is the standard deviation.

Table 3. Mean values and standard deviations of porosity and open porosity in the X, Y, Z directions for the samples of limestone of Medium Carboniferous system.

Sample	$<\phi>$	$\sigma(\phi)$	$<\phi_o>_X$	$\sigma(\phi_o)_X$	$<\phi_o>_Y$	$\sigma(\phi_o)_Y$	$<\phi_o>_Z$	$\sigma(\phi_o)_Z$
no. 7	0.1473	0.0037	0.1259	0.005	0.1269	0.0051	0.1259	0.0037
no. 25	0.1223	0.0016	0.0938	0.0023	0.0936	0.0025	0.0938	0.0029
no. 31	0.1535	0.0042	0.1388	0.0047	0.1391	0.0051	0.1392	0.0048
no. 78	0.2112	0.0032	0.205	0.0035	0.2055	0.0034	0.2052	0.0032

It is worth noting that the open porosity is practically independent of spatial direction for all samples. Furthermore, the standard deviation for the porosity estimations is less than 5%, confirming the assumption about the statistical representativity of the investigated sub-samples. Based on the obtained values of porosity and open porosity, a linear regression can be constructed:

$$\phi_o = b_1\phi + b_0,$$

where b_0 and b_1 are the scalar coefficients. Figures 2 shows such linear regressions, while their formulas obtained for each considered models are given in Table 4.

Table 4. Linear regression relating open and total porosity of sub-samples.

Sample	Open porosity X	Open porosity Y	Open porosity Z
no. 7	$1.1163\phi - 0.0386$	$1.0954\phi - 0.0345$	$1.0987\phi - 0.0345$
no. 25	$0.9834\phi - 0.0265$	$0.9824\phi - 0.0265$	$0.9825\phi - 0.0264$
no. 31	$1.0769\phi - 0.0265$	$1.0752\phi - 0.026$	$1.0721\phi - 0.0254$
no. 78	$1.0222\phi - 0.0108$	$1.0151\phi - 0.0089$	$1.0146\phi - 0.0091$

Then we numerically simulate the fluid flow through the pores for each sub-sample, calculate the absolute permeability in all spatial directions as described in the previous section and construct the following dependence of this parameter on open porosity in logarithmic scale:

$$ln(\kappa) = b_0 ln(\phi_o) + b_1,$$

where κ is the absolute permeability, b_0 and b_1 are some constants. It is clear that we can write down a slightly different functional relationship between permeability and open porosity [3,11]:

$$\kappa = e^{b_1}\phi_o^{b_0} = c\phi_o^{b_0},$$

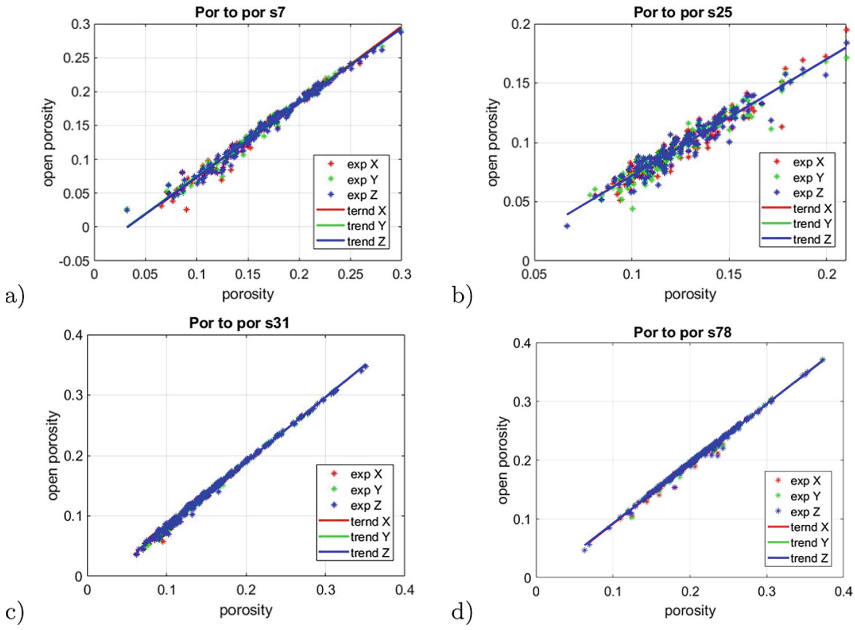


Fig. 2. Dependence of open porosity on total porosity and linear trends for the samples: a) no. 7; b) no. 25; c) no. 31; d) no. 78.

where b_0, b_1 and c are some constants. Illustrations of these dependencies are shown in the Figs. 3, 4, 5 and 6. The functional relationship between the porosity and absolute permeability for each spatial direction as well as the estimated values of the permeability for the total limestone samples are provided in Table 5. It can be seen that for all samples, the trends in different directions are very close to each other, which indicates that the samples are close to isotropic.

Table 5. Functional relationship between the open porosity and absolute permeability and the estimated values of the permeability (mD) for the total limestone samples.

Sample	Permeability X	κ_x	Permeability Y	κ_y	Permeability Z	κ_z
no. 7	$79.28\phi_o^{3.24}$	95.2	$52.58\phi_o^{3.14}$	80.3	$45.92\phi_o^{3.08}$	76.3
no. 25	$21.28\phi_o^{2.95}$	19.9	$25.41\phi_o^{3.05}$	18.4	$4.51\phi_o^{2.40}$	15.3
no. 31	$182.64\phi_o^{3.71}$	119.8	$205.23\phi_o^{4.02}$	73.5	$248.69\phi_o^{3.90}$	114.0
no. 78	$204.33\phi_o^{3.08}$	1554	$298.97\phi_o^{3.27}$	1685	$315.06\phi_o^{3.28}$	1744

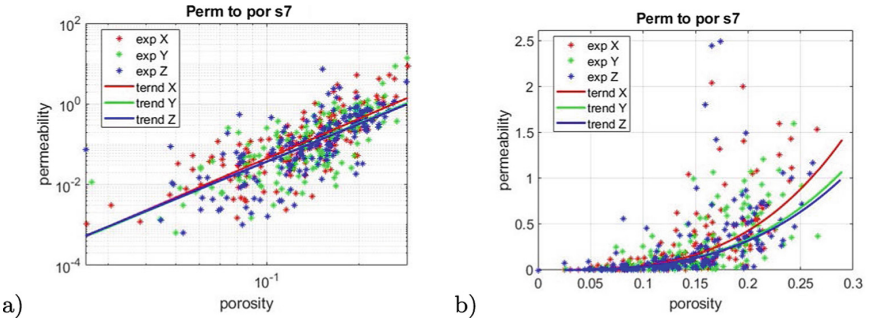


Fig. 3. Dependence of absolute permeability on porosity and trends for the sample no. 7: a) logarithmic scale; b) linear scale.

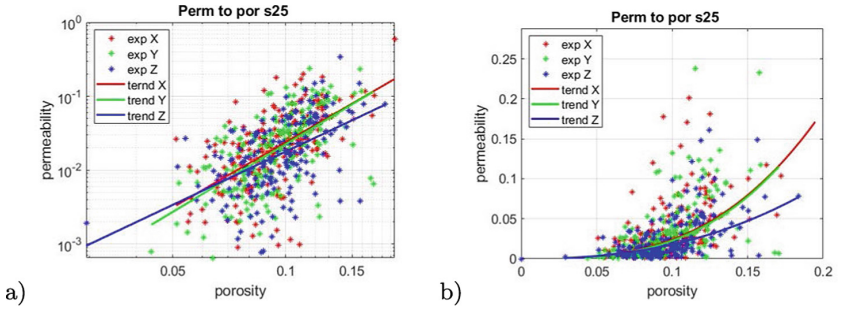


Fig. 4. Dependence of absolute permeability on porosity and trends for the sample no. 25: a) logarithmic scale; b) linear scale.

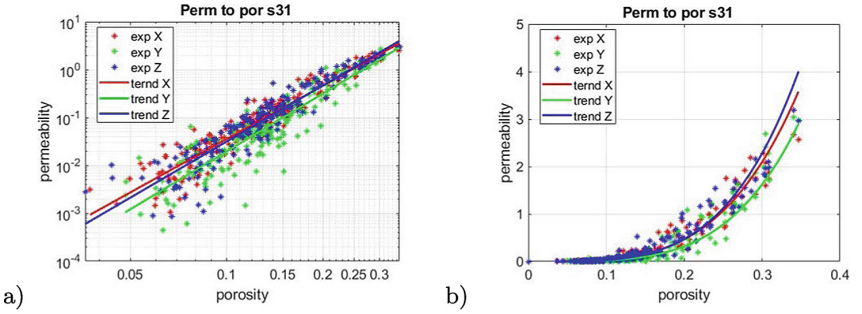


Fig. 5. Dependence of absolute permeability on porosity and trends for the sample no. 31: a) logarithmic scale; b) linear scale.

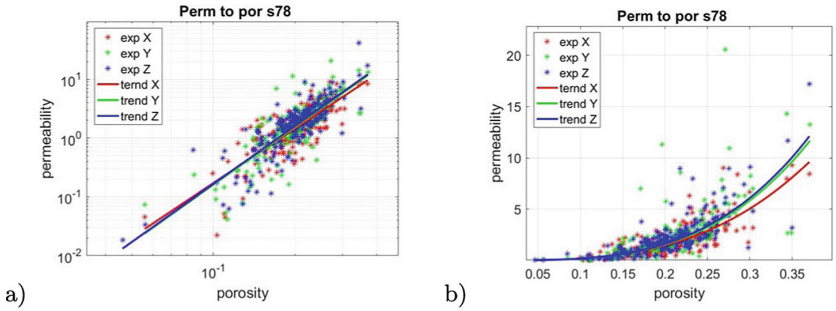


Fig. 6. Dependence of absolute permeability on porosity and trends for the sample no. 78: a) logarithmic scale; b) linear scale.

The comparison of numerical estimates with the results of laboratory experiments shows their similarity, which confirms the applicability of the proposed approach to the assessment of absolute permeability using the correlation dependence on geometry.

4 Conclusions

In this study, we presented the methodology for evaluating some basic parameters of rocks based on correlation dependence on geometry. The main idea of methodology is not to simulate fluid flows or other physical fields for the entire sample of huge size and calculate a single parameter value using supercomputers, but to use sub-samples of small but representative size for building a trend, i.e. a relation between the parameters under consideration, thus getting the ability to interpolate the simulation results to the required scale. Simulation of physical fields for small sub-images is possible using the personal computers, in our case a single desktop and nVidia GeForce 2090Ti with 12 GB of RAM was used, and it took only 10 h to calculate the permeability for 216 sub-samples. Thus, this approach can be easily used in any computational physics laboratory.

We have shown the applicability of the technique for evaluating the absolute permeability, but we assume that it can also be used when estimating other basic rock parameters: relative permeability, elastic moduli, formation factor, capillary pressure, etc. This thesis needs to be confirmed in the future.

References

1. Andra, H., et al.: Digital rock physics benchmarks - Part I: imaging and segmentation. Comput. Geosci. **50**, 25–32 (2013)
2. Andra, H., et al.: Digital rock physics benchmarks - Part II: computing effective properties. Comput. Geosci. **50**, 33–43 (2013)
3. Arns, C.H., Knackstedt, M.A., Mecke, K.R.: Characterisation of irregular spatial structures by parallel sets and integral geometric measures. Colloids Surf. A **241**(1–3), 351–372 (2004)

4. Bazaikin, Y., et al.: Effect of CT image size and resolution on the accuracy of rock property estimates. J. Geophys. Res. Solid Earth **122**(5), 3635–3647 (2017)
5. Buades, A., Coll, B., Morel, J.M.: A non-local algorithm for image denoising. In: 2005 IEEE Computer Society Conference on Computer Vision and Pattern Recognition (CVPR 2005), vol. 2, pp. 60–65 (2005)
6. Evstigneev, N.M., Ryabkov, O.I., Gerke, K.M.: Stationary stokes solver for single-phase flow in porous media: a blastingly fast solution based on algebraic multigrid method using GPU. Adv. Water Resour. **171**, 104340 (2023)
7. Gerke, K.M., Karsanina, M.V., Katsman, R.: Calculation of tensorial flow properties on pore level: exploring the influence of boundary conditions on the permeability of three-dimensional stochastic reconstructions. Phys. Rev. E **100**(5), 053312 (2019)
8. Jodra, J.L., Gurrutxaga, I., Muguerza, J., Yera, A.: Solving Poisson's equation using FFT in a GPU cluster. J. Parallel Distrib. Comput. **102**, 28–36 (2017)
9. Jouini, M.S., Vega, S., Al-Ratrout, A.: Numerical estimation of carbonate rock properties using multiscale images. Geophys. Prospect. **63**(2), 405–421 (2015)
10. Kalo, K., Grgic, D., Auvray, C., Giraud, A., Drach, B., Sevostianov, I.: Effective elastic moduli of a heterogeneous oolitic rock containing 3-D irregularly shaped pores. Int. J. Rock Mech. Min. Sci. **98**, 20–32 (2017)
11. Kameda, A., Dvorkin, J., Keehm, Y., Nur, A., Bosl, W.: Permeability-porosity transforms from small sandstone fragments. Geophysics **71**(1), N11–N19 (2006)
12. Karsanina, M.V., Gerke, K.M.: Hierarchical optimization: fast and robust multiscale stochastic reconstructions with rescaled correlation functions. Phys. Rev. Lett. **121**(26), 265501 (2018)
13. Khachkova, T., Lisitsa, V., Reshetova, G., Tcheverda, V.: GPU-based algorithm for evaluating the electrical resistivity of digital rocks. Comput. Math. Appl. **82**, 200–211 (2021)
14. Lesueur, M., Rattez, H., Colomés, O.: μct scans permeability computation with an unfitted boundary method to improve coarsening accuracy. Comput. Geosci. **166**, 105118 (2022)
15. Madonna, C., et al.: Synchrotron-based x-ray tomographic microscopy for rock physics investigations. Geophysics **78**(1), D53–D64 (2013)
16. Makarynska, D., Gurevich, B., Ciz, R., Arns, C.H., Knackstedt, M.A.: Finite element modelling of the effective elastic properties of partially saturated rocks. Comput. Geosci. **34**(6), 647–657 (2008)
17. Mostaghimi, P., Blunt, M., Bijeljic, B.: Computations of absolute permeability on micro-CT images. Math. Geosci. **45**(1), 103–125 (2013)
18. Otsu, N.: Thresholds selection method form grey-level histograms. IEEE Trans. Syst. Man Cybern. **9**(1), 1979 (1979)
19. Saenger, E.H., et al.: Analysis of high-resolution X-ray computed tomography images of bentheim sandstone under elevated confining pressures. Geophys. Prospect. **64**(4), 848–859 (2016)